

PAPER • OPEN ACCESS

In situ NAP-XPS spectroscopy during methane dry reforming on ZrO₂/Pt(1 1 1) inverse model catalyst

To cite this article: C Rameshan *et al* 2018 *J. Phys.: Condens. Matter* **30** 264007

View the [article online](#) for updates and enhancements.

Related content

- [Spectroscopic studies of surface–gas interactions and catalyst restructuring at ambient pressure: mind the gap!](#)
Günther Rupprechter and Christian Weilach
- [Ambient pressure photoelectron spectroscopy: Practical considerations and experimental frontiers](#)
Lena Trotochaud, Ashley R Head, Osman Karsliolu *et al.*
- [Synchrotron radiation application on model catalyst surfaces](#)
S Surnev, M G Ramsey and F P Netzer



IOP | ebooks™

Bringing you innovative digital publishing with leading voices to create your essential collection of books in STEM research.

Start exploring the collection - download the first chapter of every title for free.

In situ NAP-XPS spectroscopy during methane dry reforming on ZrO₂/Pt(1 1 1) inverse model catalyst

C Rameshan¹, H Li¹, K Anic¹, M Roiaz¹, V Pramhaas¹, R Rameshan^{1,2}, R Blume², M Hävecker², J Knudsen³, A Knop-Gericke² and G Rupprechter¹

¹ Institute of Materials Chemistry, Technische Universität Wien, Vienna, Austria

² Department of Inorganic Chemistry, Fritz Haber Institute of the Max Planck Society, Berlin, Germany

³ Division of Synchrotron Radiation Research and the MAX IV Laboratory, Lund University, Lund, Sweden

E-mail: christoph.rameshan@tuwien.ac.at and guenther.rupprechter@tuwien.ac.at

Received 8 March 2018, revised 9 May 2018

Accepted for publication 22 May 2018

Published 8 June 2018




CrossMark

Abstract

Due to the need of sustainable energy sources, methane dry reforming is a useful reaction for conversion of the greenhouse gases CH₄ and CO₂ to synthesis gas (CO + H₂). Syngas is the basis for a wide range of commodity chemicals and can be utilized for fuel production via Fischer–Tropsch synthesis. The current study focuses on spectroscopic investigations of the surface and reaction properties of a ZrO₂/Pt inverse model catalyst, i.e. ZrO₂ particles (islands) grown on a Pt(1 1 1) single crystal, with emphasis on *in situ* near ambient pressure x-ray photoelectron spectroscopy (NAP-XPS) during MDR reaction. In comparison to technological systems, model catalysts facilitate characterization of the surface (oxidation) state, surface adsorbates, and the role of the metal-support interface. Using XPS and infrared reflection absorption spectroscopy we demonstrated that under reducing conditions (UHV or CH₄) the ZrO₂ particles transformed to an ultrathin ZrO₂ film that started to cover (wet) the Pt surface in an SMSI-like fashion, paralleled by a decrease in surface/interface oxygen. In contrast, (more oxidizing) dry reforming conditions with a 1:1 ratio of CH₄ and CO₂ were stabilizing the ZrO₂ particles on the model catalyst surface (or were even reversing the strong metal support interaction (SMSI) effect), as revealed by *in situ* XPS. Carbon deposits resulting from CH₄ dissociation were easily removed by CO₂ or by switching to dry reforming conditions (673–873 K). Thus, at these temperatures the active Pt surface remained free of carbon deposits, also preserving the ZrO₂/Pt interface.

Keywords: inverse model catalyst, *in situ* XPS, methane dry reforming, surface structure, catalysis, IRAS, strong metal-support interaction (SMSI)

 Supplementary material for this article is available [online](#)

(Some figures may appear in colour only in the online journal)



Original content from this work may be used under the terms of the [Creative Commons Attribution 3.0 licence](#). Any further distribution of this work must maintain attribution to the author(s) and the title of the work, journal citation and DOI.

1. Introduction

Fossil fuels still represent the major energy source of the globalized economy and the annually growing consumption creates great environmental challenges due to increasing levels of greenhouse gases [1, 2]. Methane and carbon dioxide constitute a major part of greenhouse emissions with strong impact on global warming [3]. Since fossil fuels are limited there are great efforts in finding new, renewable and sustainable energy sources [4]. The conversion of small carbon containing molecules such as CH₄ to syngas (mixture of CO and H₂) may be part of possible solutions. Syngas is a building block for valuable liquid fuels and chemicals such as longer chain hydrocarbons produced by the Fischer–Tropsch (FT) process, or for synthesis of methanol and dimethylether [5–7].

The industrially relevant processes for syngas production include methane steam reforming, partial oxidation of methane with oxygen or air, and methane dry reforming (MDR) with carbon dioxide [3, 8]. Methane steam reforming produces a H₂/CO ratio of 3 [9] that is higher than that required for FT or methanol synthesis (H₂/CO = 2) [10]. Partial methane oxidation (H₂/CO = 2) is favourable for production of heavier hydrocarbons and naphtha [11] and has high conversion rates and high selectivity [12], but the exothermic nature of the reaction has drawbacks (e.g. heat removal) [8].

Dry reforming of methane (CH₄ + CO₂ → 2CO + 2H₂) has several environmental benefits: it can utilize biogas as source [13, 14] (biogas from anaerobic decomposition of organic material produces nearly equal CH₄ and CO₂ concentrations [15]) and, more importantly, it reduces emissions of greenhouse gases CH₄ and CO₂ by transforming them into value-added syngas [16]. Natural gas with a high CO₂ content can also be transformed into fuel via MDR [5]. The lower syngas ratio (H₂/CO = 1) of MDR is suitable for the synthesis of oxygenated chemicals [17] and hydrocarbons from FT synthesis. MDR has also been considered as a suitable route to thermochemically convert solar energy to fuel [18, 19]. Ross reported that MDR has 20% lower operating costs than the other CH₄ reforming processes [20]. Therefore, we have focused on MDR in the current study.

The most widely used metal for MDR is Ni [21–25], but Ni-based catalysts often undergo severe deactivation (loss of activity) with time, due to carbon deposition (carbon nanotube formation) [3, 26, 27]. When using noble metal catalysts, the coking problem can be avoided or reduced. Therefore, MDR has been studied over a series of supported Pt, Pd, Rh, and Ru catalysts [1, 28–34] but also Co and Fe have been investigated [3, 16]. In terms of performance, Németh *et al* demonstrated comparable catalytic activity of Ni–ZrO₂ and Pt–ZrO₂ powder catalysts (1 wt% metal) [35]. However, an apparent drawback of noble metal systems is their high cost. A possible solution is the addition of small amounts of noble metals (Rh, Ru, Pd, and Pt) to Ni catalysts, which leads to improved catalytic properties and lower sensitivity to carbon deposition, while maintaining a low materials cost [3, 36]. Furthermore, the use of bimetallic nanoparticles may also improve the catalytic performance [1, 3, 37–39].

As controversially discussed in the literature, the mechanism of MDR seems bi-functional. CH₄ is activated on the metal via dissociation [40], whereas CO₂ is activated on acidic/basic supports. On acidic supports, CO₂ is activated via formation of formates (reaction with the surface hydroxyls) and on basic supports by forming oxy-carbonates [41, 42]. For catalysts with relatively inert supports like SiO₂ the mechanism is considered to follow a mono-functional pathway, with only the metal activating both reactants [1, 3]. Apart from the different possible reaction pathways, the role of the metal-oxide interface has been vividly discussed [41, 43, 44].

Clearly, microscopic mechanisms of the interplay of metal and support, including potential structure changes under reaction conditions (e.g. SMSI, and the resulting loss of activity) [45, 46], need to be better understood, e.g. by utilizing a surface science approach.

Based on this motivation we have carried out a systematic surface-sensitive study of the interaction of CH₄/CO₂ with an inverse model catalyst, i.e. ZrO₂ particles/islands supported on a Pt(1 1 1) single crystal (also using Pt(1 1 1) as a support-free reference). Inverse model catalyst surfaces allow—when compared to powder systems—better spectroscopic identification of the surface state, metal-support interactions and the role of the interface [47]. Accordingly, the ZrO₂/Pt(1 1 1) model catalyst was characterized by temperature programmed desorption (TPD), infrared spectroscopy (IRAS), and x-ray photoelectron spectroscopy (XPS) (the latter also applied *in situ* during catalytic reaction).

2. Experimental

2.1. Laboratory measurements

The laboratory measurements (TPD and IRAS) were performed in a custom-built UHV chamber that was described elsewhere [48–50]. The preparation chamber is equipped with a differentially-pumped quadrupole mass spectrometer (MKS eVison+), LEED optics (SPECS ERLEED 1000-A), and a standard x-ray source (SPECS XR 50, with AlK α and MgK α anode) combined with a SPECS EA 150 PHOIBOS hemispherical analyzer. The UHV-compatible high pressure cell ('Rupprechter design') [50, 51] is connected to a Fourier transform IR spectrometer (Bruker Vertex 60v) and a ZnSe photoelastic modulator operating at 34 kHz.

The Pt(1 1 1) single crystal (MaTek) was cleaned by sputtering with 1 kV Ar⁺ ions (p Ar = 5 × 10⁻⁶ mbar, sputtering current = 2 μ A) for 45 min followed by thermal annealing to 1070 K. Crystal cleanliness was confirmed by XPS. For the inverse model system, ZrO₂ particles were prepared on the Pt(1 1 1) single crystal by sputter deposition of Zr (from a foil, Alfa Aesar, purity 99.5%) in 5 × 10⁻⁶ mbar O₂ at RT, utilizing a custom-built sputter source for precise and reproducible deposition amounts [52]. The nominal thickness of the as-deposited ZrO₂ film was 0.3 nm (the thickness of a (1 1 1) oriented bulk ZrO₂ (O–Zr–O) layer is 0.295 nm [53]). Sputter deposition by this special technique leads to the growth of uniformly distributed ZrO₂ islands, as observed by scanning

tunneling microscopy (STM) [54]. Directly after deposition, the sample was annealed in 5×10^{-7} mbar O_2 to 873 K to fully oxidize the deposited ZrO_x to ZrO_2 leading to the formation of larger ZrO_2 islands on Pt(1 1 1). As shown in the following section, the coverage of the ZrO_2 islands on Pt(1 1 1) was about half of a monolayer. Based on the nominally deposited 0.3 nm (monolayer), this would result in ZrO_2 islands with an average thickness of two oxide layers (double layer O–Zr–O–Zr–O). All experiments (lab and synchrotron) were performed on the same sample.

Only high purity gases from Messer Austria were used for all experiments. The purity of oxygen and hydrogen was 5.0, CO_2 was 4.8, CH_4 was 4.5 and the purity of CO was 4.7. Additionally, in order to avoid carbonyl contaminations, a carbonyl absorber cartridge was installed in the CO gasline [49].

Experiments in the low pressure range were performed both in the UHV preparation chamber and high pressure cell. Dosing of gases was carried out using a high precision leak valve. The Langmuir coverage was calculated assuming a sticking coefficient of unity. The IRAS measurements of CO adsorption were carried out under UHV in the high pressure cell (spectral range 1500–2600 cm^{-1}). Data processing was performed according to procedures described by Hollins [55].

TPD spectra were collected by a differentially-pumped MKS eVision+ quadrupole mass spectrometer, and temperature ramping was performed by a Eurotherm 3216 PID controller, with a heating rate of 60 K min^{-1} [53].

The ability to regenerate ZrO_2 particles after exposure to air was confirmed prior to the synchrotron measurements. This was important as the sample was prepared in the Vienna lab and then transported to the respective synchrotron facility. For this, the sample was removed from the UHV chamber and exposed to air for 24–48 h. Afterwards, the same sample was again mounted to the manipulator of the UHV chamber. After a reoxidation cycle, the original chemical composition and surface structure of the ZrO_2 islands was re-established, as confirmed by XPS and TPD.

2.2. Synchrotron measurements

The MDR *in situ* experiments were conducted at two different synchrotron facilities due to different experimental requirements. The ISISS end station at HZB/BESSY II is capable to run *in situ* experiments up to 1000 K, which is required for the MDR catalytic measurements. However, the system is not optimized for true UHV studies (i.e. the base pressure of the *in situ* cell is only in the mid 10^{-8} mbar range). In comparison, the SPECIES end station at the MAX IV laboratory is limited to a maximum reaction temperature of 673 K, which is below real dry reforming operational temperatures. However, the special design of this system allows true UHV investigations and (clean) *in situ* experiments. This is important for the characterisation of the as-prepared state of the model catalyst and the initial exposure to the reactive gas environment. Nevertheless, benchmark experiments ensured that the experimental results of both beamlines were compatible.

2.3. Bessy setup

In situ experiments were performed at the ISISS beam line of the HZB/BESSY II synchrotron in Berlin with a near-ambient pressure high energy x-ray photoelectron spectroscopy (NAPHE-XPS) setup, which enables measurements at elevated pressures (up to 7 mbar) with photon energies ranging from ~80 up to 2000 eV. The main parts are a ‘high pressure’ chamber with an attached differentially-pumped hemispherical analyser (modified SPECS Phoibos 150) including a 2D delay line detector. A detailed description of the near-ambient pressure XPS-setup is given in [56]. Samples were heated via a tantalum back sheet using an infrared laser. The temperature was monitored with a pyrometer measuring the surface temperature, as well as by a thermocouple.

2.4. MAX IV setup

In situ near ambient pressure x-ray photoelectron spectroscopy (NAP-XPS) was performed at the high resolution XPS endstation SPECIES at the MAX IV Laboratory. The setup and beamline is described in detail in [57, 58]. Again, photon energies from ~80 to 2000 eV could be chosen. The system was capable of performing ambient pressure and true UHV experiments. This is realized by using a retractable ‘high-pressure cell’, which can be docked to the front aperture of the SPECS PHOIBOS 150 NAP analyser for ambient pressure experiments. During *in situ* measurements only the cell was filled with gases, while the analysis chamber remained evacuated. Heating was achieved through electron bombardment of the vacuum side of the wall behind the sample seat of the high-pressure cell. With this design no hot filament was exposed to the gas environment. The sample temperature was measured with a chromel-alumel thermocouple wire pair mounted on the transferable sample holder.

Both *in situ* setups are designed as continuous catalytic flow cells with gas analysis by mass spectrometry. For catalytic reactions, the interaction of the model catalysts surface with pure CH_4 or CO_2 was studied first (0.1 mbar in both cases). For the MDR reaction a total pressure of 0.2 mbar with 1:1 composition of CH_4 and CO_2 was used (during the single bunch beamtime higher pressures were not accessible). During reaction the temperature was varied stepwise from RT to 873 K. Reaction educts and products were followed by mass spectrometry. Additionally, a clean Pt(1 1 1) single crystal was used as reference for the MDR reaction and for peak assignments.

Surface sensitive *in situ* XPS spectra were obtained with different incident photon energies (140 eV for VB, 210 eV for Pt 4f, 320 eV for Zr 3d, 420 eV for C 1s, and 670 eV for O 1s). These correspond to kinetic photoelectron energies between 130 and 150 eV, which leads to almost equal information depth (inelastic mean free path, IMFP) of 0.5–0.6 nm, according to NIST Standard Reference Database [59]. In case of depth profiling measurements, the photon energies were increased in multiple steps, resulting in photoelectron energies up to 740 eV, and an information depth (IMFP) up to 1.5 nm. After

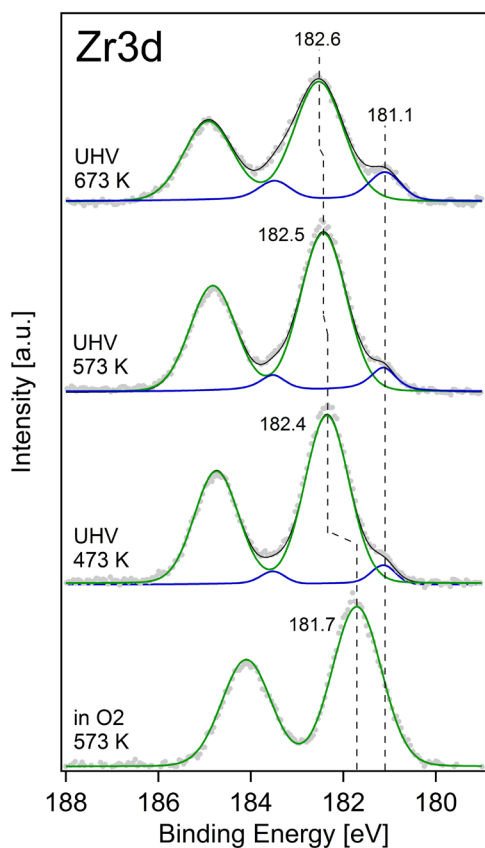


Figure 1. Zr 3d spectra of the as-deposited and oxidized ZrO₂ nanoparticles ($p(\text{O}_2) = 4.5 \times 10^{-5}$ mbar) and after stepwise annealing to 673 K in UHV. With increasing temperature, the evolution of an increasing Zr film signal at 181.1 eV was observed.

each change of excitation energy a spectrum of the Fermi edge was recorded for calibration of the binding energy axis. All spectra were referenced to the Fermi edge, which is necessary due to monochromator mechanics at the synchrotron [60].

The spectra were fitted with CasaXPS, using a Shirley background subtraction and mixed Gaussian–Lorentzian (GL) peak shapes for the Zr, C, and O components. The Zr 3d region was fitted with doublets, restricted by equal FWHM, fixed doublet separation of 2.4 eV (spin orbit splitting) and an area ratio of 2:3 [53]. The assignment of the signals to Zr-clusters and Zr-film was based on previous studies by Li *et al* [53]. For the Pt 4f signal an asymmetry function was used for peak fitting. The parameters for the asymmetry were obtained from measuring the clean Pt(1 1 1) reference sample. The Pt 4f signal was fitted with doublets with a fixed separation of 3.3 eV and an area ratio of 3:4.

Possible beam damage or beam-induced surface modifications were examined prior to the actual *in situ* experiments. This was achieved by measuring different positions (spots) on the sample surface (in equilibrium gas pressure) upon using different beam exposure times [60]. Based on the comparison of the results, which indicated no differences for different exposure times, x-ray beam damage could be excluded.

Additional *in situ* measurements were carried out on a Pt(1 1 1) single crystal, for comparison with the inverse model system and for providing reference data for fitting.

3. Results

3.1. Structural characterisation by XPS, IR and TPD

Prior to the actual MDR experiments, a detailed characterisation of the as-prepared (oxidized) and annealed ZrO₂/Pt(1 1 1) inverse model catalyst surface was carried out to determine structure and thermal stability in UHV. Accordingly, the ZrO₂/Pt(1 1 1) system was heated stepwise to 673 K in UHV while measuring surface-sensitive XPS spectra at MAX IV (figure 1).

In 4.5×10^{-5} mbar O₂ at 573 K a distinct Zr 3d feature could be observed at 181.7 eV (figure 1), which agrees with values reported for supported ZrO₂ with cluster-like structure [53, 61]. The Zr 3d signal was slightly shifted to lower binding energies (BE), presumably due to the presence of adsorbed oxygen, see the detailed discussion below (section 3.2 *in situ* XPS). Upon pumping off the O₂ background at RT and heating the model catalyst to 473 K in UHV, the main ZrO₂ signal shifted to 182.4 eV (expected for ZrO₂ islands), and an additional component appeared at 181.1 eV (figure 1). The peak shift of the main signal was likely caused by desorption of adsorbed oxygen. In line with our previous studies on supported thin ZrO₂ films the species at 181.1 eV can be attributed to the growth of an ultrathin ZrO₂ film on the Pt(1 1 1) surface (i.e. only one tri-layer of ZrO₂) [53] (see also the model in the discussion section). The 0.4 eV lower BE of the tri-layer in our previous study can be explained by the different substrate materials (Pt versus Pt₃Zr) and the different morphology (islands versus continuous film). The driving force of film growth is that at elevated temperatures and in UHV the ultrathin ZrO₂ film is thermodynamically more stable than thicker ZrO₂ nanoparticles or clusters [53, 62] (up to the point when the oxide decomposes, >1173 K [63]). When the temperature was raised to 573 and 673 K in UHV (figure 1), the ZrO₂ trilayer film signal further increased (i.e. up to ~20% of the Zr 3d signal at 673 K), while the intensity of the cluster-related signal decreased. The formation of a PtZr alloy during annealing could not be observed, as the expected signal at 179.6 eV was absent (see figure 1) [53]. Also, the Pt 4f signal did not change during UHV annealing to 673 K (see supporting information figure S1 (stacks.iop.org/JPhysCM/30/264007/mmedia)). Upon reoxidation in O₂ atmosphere ($p = 4.5 \times 10^{-5}$ mbar, 573 K, 10 min), the initial state of the surface with only ZrO₂ islands (on average a double-layer) was regenerated, i.e. the observed spreading of ZrO₂ on Pt(1 1 1) was reversible.

To learn more about the structure of the ZrO₂/Pt(1 1 1) inverse model catalyst, infrared measurements were performed, using CO as probe molecule (figure 2(a)). After exposure of the (oxidized) inverse model catalyst surface to 4L CO at RT, a distinct feature at 2090 cm⁻¹ was observed, characteristic of on-top CO adsorbed on the uncovered Pt(1 1 1) surface [64] (CO does not adsorb on the ZrO₂ surface at these conditions [53]). To quantify the amount of adsorbed CO, TPD spectra were acquired after 4L CO were dosed to the sample surface at 300 K (figure 2(b)). A desorption feature with a peak maximum at ~390 K originating from Pt(1 1 1) was observed [65]

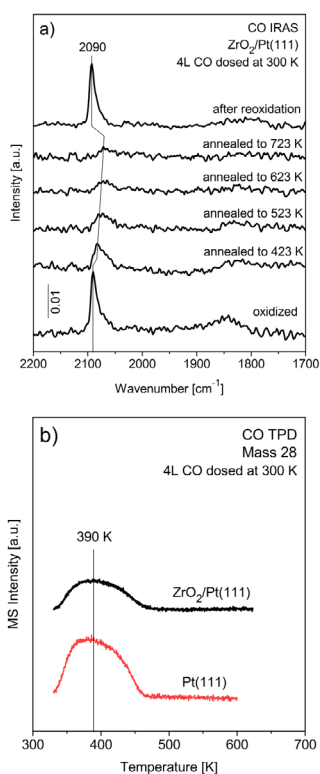


Figure 2. (a) Infrared spectra after exposure of 4L CO to the as-prepared (oxidized) and UHV-annealed ZrO_2 nanoparticles on Pt(111). The signal of on-top CO is decreasing with increasing annealing temperature. The initial spectrum with a signal at 2090 cm^{-1} can be retrieved after reoxidation of the inverse model catalyst surface. (b) CO TPD spectra upon exposure to 4L CO at 300 K. The bottom spectrum (red) shows desorption from a clean Pt(111) surface (0.5 ML coverage) as reference. The top TPD spectrum (black) was collected from the as-prepared and oxidized $\text{ZrO}_2/\text{Pt}(111)$ sample.

(corresponding to a desorption energy of $\sim 98\text{ kJ mol}^{-1}$). By comparison with the area of desorption from the clean Pt(111) surface (with a CO saturation coverage of 0.5 ML at 300 K), it can be estimated that $\sim 50\%$ of the Pt surface was covered by the ZrO_2 nanoparticles/islands. Accordingly, these islands must be $\sim 0.6\text{ nm}$ in thickness but their average size is currently unknown (note that Lackner *et al* reported the growth of small islands (about 2–5 nm in size) when depositing ZrO_2 by the same method on a Rh(111) single crystal [54]).

Upon annealing $\text{ZrO}_2/\text{Pt}(111)$ in UHV to 423 K (figure 2(a)) and re-dosing 4L CO at RT, the amount of adsorbed CO was reduced and shifted to lower wavenumber ($\sim 2080\text{ cm}^{-1}$). This is in line with XPS spectra (figure 1), indicating the onset of formation of an ultrathin ZrO_2 layer wetting the Pt(111) surface and therefore blocking adsorption sites. The redshift may be due to lower CO coverage and/or lower CO ordering (that would cause reduced dipole–dipole-interaction) [65–67]. A roughening of the Pt surface (that would also cause a redshift of CO) is also possible [68].

When the surface was heated to even higher temperatures (523, 623 and 723 K) the CO signal intensity decreased further, until it was nearly indistinguishable from the background

noise. At the highest temperature, the signal shifted down to 2070 cm^{-1} . Again, this is in line with the increasing signal of the spreading ultrathin ZrO_2 film covering more and more of the Pt(111) surface. After this series of IR spectra, the model catalyst surface was reoxidised and again exposed to 4L CO at RT (figure 2(a), top spectrum). The obtained infrared signal was comparable to the initial signal after model catalyst preparation, with a peak at 2090 cm^{-1} of similar signal intensity. The XPS and infrared data point to the conclusion that upon UHV annealing (reduction) the ZrO_2 islands started to wet the Pt surface, whereas exposure of the inverse model catalyst to oxidising conditions re-established the ZrO_2 islands/clusters and the initial amount of uncovered Pt(111). This is an important finding, because it is essential to know whether under dry reforming reaction conditions the ZrO_2 islands may wet/cover the Pt(111) surface, causing a pronounced surface modification of the catalyst (that may be beneficial or detrimental for the catalytic performance).

3.2. *In situ* NAP XPS studies

Before the actual MDR experiments, the interaction of the inverse model catalyst surface with the individual reactants (i.e. with CH_4 or CO_2 separately) was tested. This provides useful information on the reactivity of the respective molecule on the surface and its temperature-dependent effect on the surface structure/composition.

3.2.1. CH_4 exposure to $\text{ZrO}_2/\text{Pt}(111)$. Figure 3 summarizes the *in situ* XPS results for exposure to 0.1 mbar CH_4 at increasing temperature (measured at BESSY II).

For the pristine model catalyst surface (regenerated at 673 K in 4.5×10^{-5} mbar O_2) the binding energies are 181.7 eV for Zr 3d, corresponding to the ZrO_2 particles/islands, and 71 eV for Pt 4f of the Pt(111) substrate (metallic Pt) [69]. No carbon traces were observed on the surface. Upon dosing of 0.1 mbar CH_4 at 673 K the signal of the ZrO_2 clusters shifted to 182.3 eV. A similar shift was observed in the O 1s signal, whereas the Pt 4f signal stayed at 71 eV.

To explain the binding energy shift of the Zr 3d and O 1s signals a closer look on the O 1s peak components is needed (note that the peak fitting for O 1s is strongly simplified as multiple factors have to be considered, see the supporting information for a detailed discussion). Upon oxidative treatment two components could be observed: a low BE component at $\sim 529.2\text{ eV}$ (blue, figure 3) whose intensity turned out to be rather unaffected by the atmosphere (pointing to a ‘island-bulk like’ ZrO_2), and a high BE component at $\sim 530.1\text{ eV}$ (green), whose intensity depended on the atmosphere (pointing to surface or interface oxygen species that can be removed or replenished; e.g. O from ZrO_2 at the interface with possible charge transfer from O to Pt support [70, 71]). Upon switching from O_2 to CH_4 atmosphere, which produces C and H on the free Pt surface, the surface/interface oxygen vanished, leading to a decrease in intensity of the high BE (530.7 eV, green) component.

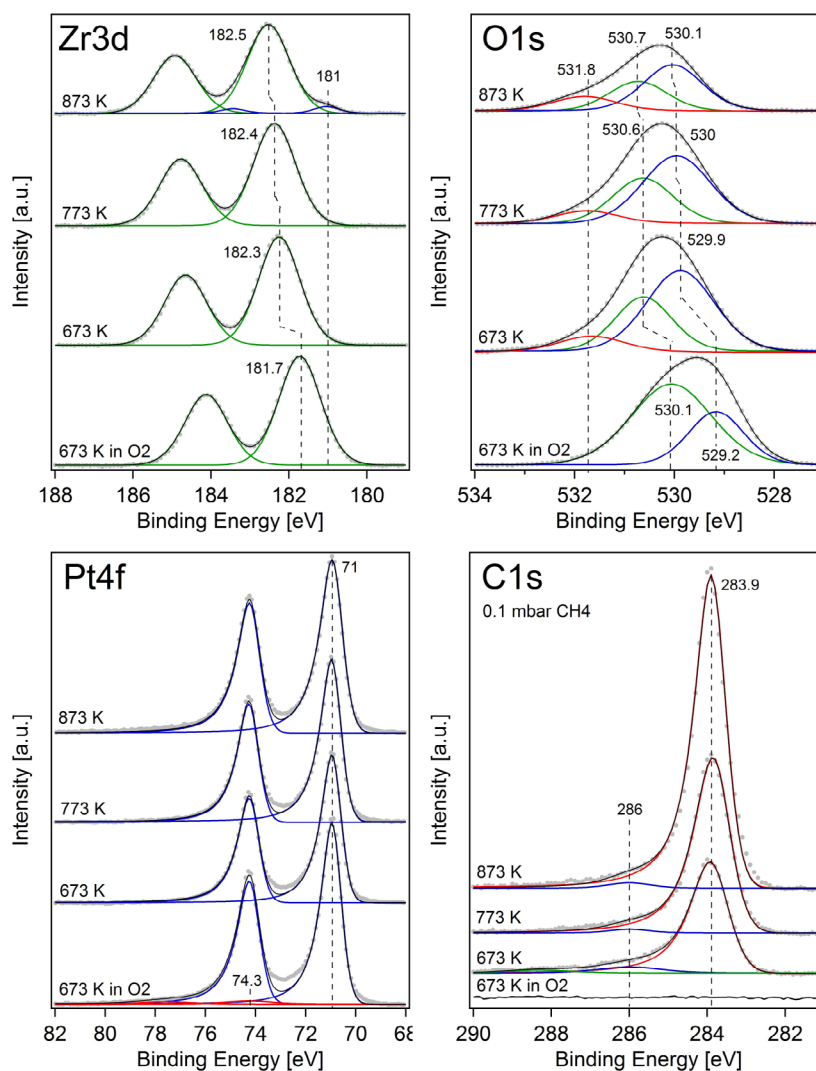


Figure 3. *In situ* XPS spectra of the $\text{ZrO}_2/\text{Pt}(111)$ inverse model catalyst during 0.1 mbar CH_4 exposure at increasing reaction temperature. The bottom spectra were recorded prior to CH_4 exposure in $p(\text{O}_2) = 4.5 \times 10^{-5}$ mbar at 673 K.

Note that at the same time the entire O 1s and Zr 3d signals shifted to higher BE. With increasing temperature, the Zr 3d signal shifted even more whereas O 1s did not. When comparing the O 1s spectra of the experiments described below (pure CO_2 , switching from CH_4 to CO_2 and dry reforming with CO_2/CH_4) a clear trend can be identified. For oxygen-rich/oxidizing conditions an increased intensity of the high BE component (green) can be found and additionally a total shift of Zr 3d and O 1s to lower BE is observed. In contrast, for reducing conditions (UHV or CH_4) the intensity of the high BE component of O 1s was much lower and peaks of O, Zr were located at higher BE. For the initial state of the (oxidized) model catalyst surface or for more oxidizing reaction conditions, we can thus propose that the higher abundance of surface/interface oxygen lead to a relative downshift of the O 1s and Zr 3d signals. For reducing conditions (UHV, CH_4), less surface/interface oxygen is present and thus the Zr 3d and O 1s signals are located at the expected values. Following this discussion, Norton *et al* reported that the surface work function depends on the coverage of adsorbate molecules, as shown for CO adsorption on $\text{Pt}(111)$ [72].

In the C 1s spectra the formation of graphitic carbon (283.9 eV) was observed at 673 K. Also, trace amounts of carbonylic/carboxylic species (286 eV) were present with a corresponding component in the O 1s spectra at 531.8 eV. These carbon species result from the dehydrogenation of CH_4 on Pt [73] and reaction of C/ CH_x species with surface oxygen. Similarly, Fuhrmann *et al* showed that upon CH_4 adsorption and dehydrogenation on $\text{Pt}(111)$ above 550 K the dominant species formed was graphitic carbon [74]. For the oxidized surface (673 K, $p(\text{O}_2) = 4.5 \times 10^{-5}$ mbar) trace amounts of PtO_x (74.3 eV) were also observed in the Pt 4f spectra, which vanished upon CH_4 exposure.

Upon raising the temperature to 773 K, the amount of graphitic carbon on the surface increased, as more CH_4 was dehydrogenated to carbon. In the Zr 3d signal, a small shift to 182.4 eV was observed, whereas the Pt 4f and O 1s spectra did not change significantly. At the highest temperature (873 K) the amount of surface carbon drastically increased. Also, the Zr 3d signal showed some major changes. Again, the signal of the ZrO_2 clusters shifted further to higher BE (182.5 eV), and the evolution of a new small signal at 181 eV was observed.

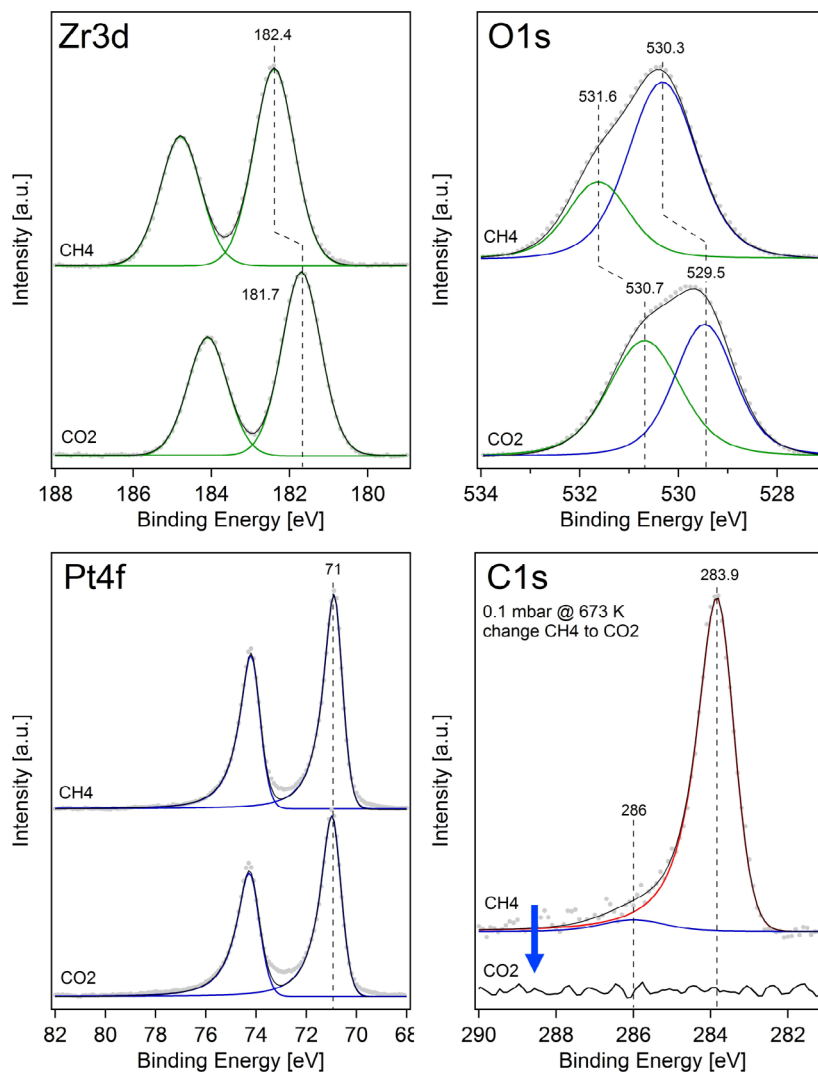


Figure 4. *In situ* XPS spectra of the $\text{ZrO}_2/\text{Pt}(111)$ inverse model catalyst while switching from 0.1 mbar CH_4 to 0.1 mbar CO_2 at 673 K. A complete removal of the carbon species was observed.

As already described in the previous section, this results from the formation of small patches of a ZrO_2 trilayer film on the surface [53]. Again, the Pt 4f signal did not change, excluding the formation of a PtZr alloy or other changes of the substrate material (see supporting information for further discussion on the limits of spectral resolution for Pt 4f). When switching back to oxidative conditions (673 K in 4.5×10^{-5} mbar O_2), as before CH_4 exposure, the signals of Zr 3d and O 1s shifted back to their initial state and all carbon was removed from the surface.

3.2.2. CO_2 exposure to $\text{ZrO}_2/\text{Pt}(111)$. In the next step, the interaction of CO_2 with the $\text{ZrO}_2/\text{Pt}(111)$ model catalyst surface was studied by introducing 0.1 mbar CO_2 into the *in situ* XPS cell at 673 K, followed by increasing the temperature step-wise to 873 K while measuring *in situ* XPS spectra. Similar to the CH_4 experiment, the position of the Zr 3d signal before CO_2 exposure was at 181.8 eV. However, the CO_2 atmosphere caused no significant change of the Zr 3d peak position and composition for all temperatures (673, 773 and 873 K, see

supporting information figure S2). Compared to exposure to pure CH_4 , the formation of a ZrO_2 trilayer film at 873 K was not observed, indicating that CO_2 stabilized the cluster structure (i.e. the gas atmosphere has a rather oxidizing potential, which maintains the particle structure). Additionally, no significant changes were observed for C 1s, O 1s and Pt 4f. No carbon formation occurred at all temperatures and the Pt 4f signal was constant at 71 eV. The peak maxima of O 1s stayed between 529.6 and 529.8 eV without major changes of the peak shape. This leads to the conclusion that CO_2 did not alter the model catalyst surface (and did not remove surface/interface oxygen), but it seems to have a stabilizing effect on the ZrO_2 particles (see also the model in figure 6). As shown in the previous section (figure 1), in UHV the formation of the ZrO_2 ultrathin film was observed already at 473 K.

3.2.3. $\text{CH}_4 + \text{CO}_2$ switching on $\text{ZrO}_2/\text{Pt}(111)$. Following the studies of the interaction with the individual reactants, we have examined the effect of switching from 0.1 mbar CH_4 (mainly leading to carbon formation on the surface) to

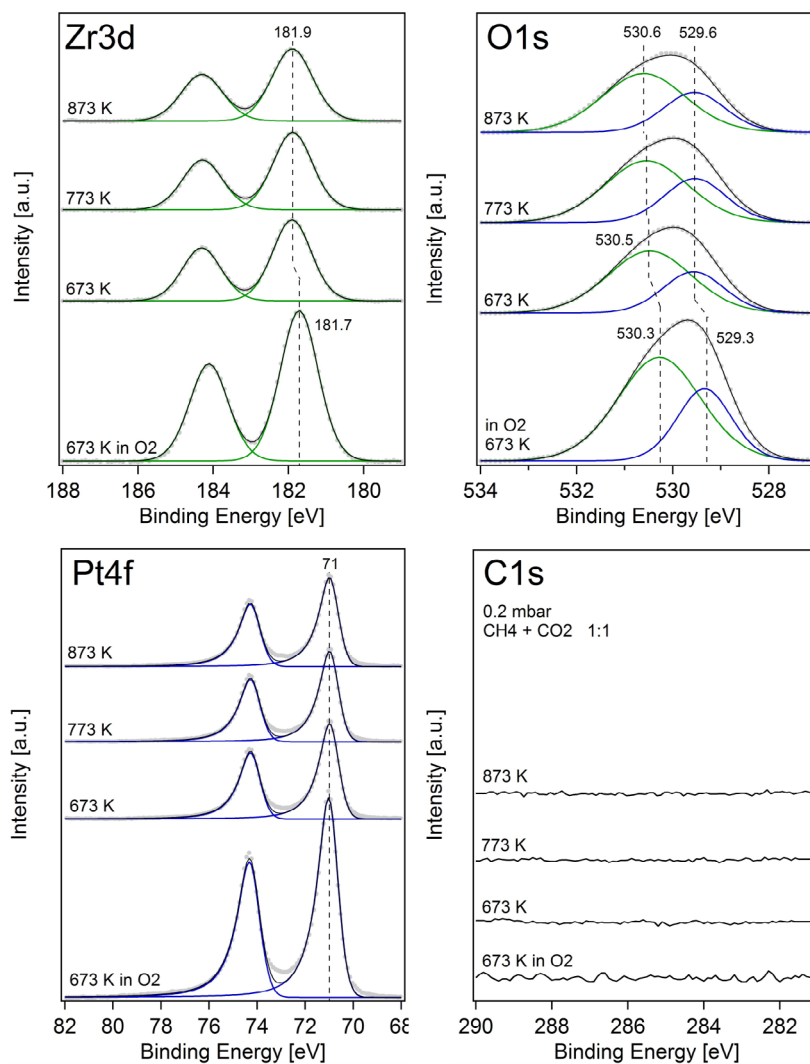


Figure 5. *In situ* XPS spectra of the $\text{ZrO}_2/\text{Pt}(111)$ inverse model catalyst during MDR reaction (flow of 0.1 mbar CH_4 + 0.1 mbar CO_2) at increasing reaction temperature. The bottom spectra were recorded in oxygen environment (673 K, $p(\text{O}_2) = 4.7 \times 10^{-5}$ mbar), prior to exposure to the reaction mixture.

0.1 mbar of CO_2 . As shown in figure 4, the entire C 1s signal immediately vanished after switching from CH_4 to CO_2 atmosphere at 673 K.

The pathway for surface carbon removal under these conditions is via the Boudouard-reaction ($\text{C} + \text{CO}_2 \rightarrow 2\text{CO}$) with CO_2 reacting with the surface carbon [75]. For MDR on noble metal catalysts, Qin *et al* also reported the efficient removal of surface carbon via this pathway for Rh, Ru, Ir, Pd and Pt supported on MgO [76].

When changing from (reducing) CH_4 to CO_2 the Zr 3d signal shifted from 182.4 to 181.7 eV and the O 1s spectra shifted from 530.3 (531.6) to 529.5 (530.7) eV. Apparently, CO_2 has an oxidizing effect ($\text{CO}_2 \rightarrow \text{CO} + \text{O}$), most likely via CO_2 activation at the ZrO_2/Pt interface and/or the (reduced) ZrO_2 islands. This leads to re-oxidation of the reduced surface/interface sites, as deduced from the strong intensity increase of the O1s component at higher BE (green) upon changing from reducing (CH_4) to more oxidizing conditions (CO_2). This is attributed to the changing gas phase and the resulting surface work function change of the ZrO_2 particles,

as discussed above. The Pt 4f signal was not affected with a constant peak position at 71 eV.

Reference measurements on pure Pt(111) (see supporting information S3) showed that the removal of surface carbon by CO_2 also occurs in the absence of the ZrO_2 particles/islands, indicating that Pt is catalysing the carbon removal by CO_2 . Unfortunately, the amount of surface carbon was too low to obtain meaningful catalytic data (by CO mass spectrometer detection) to clarify whether the ZrO_2 support has an additional promoting effect on CO_2 activation and on carbon removal.

3.2.4. $\text{CH}_4 + \text{CO}_2$ mixture on $\text{ZrO}_2/\text{Pt}(111)$. After static and switching studies of the individual reactants, the actual MDR reaction was examined *in situ*. Following the usual oxidative treatment of the $\text{ZrO}_2/\text{Pt}(111)$ inverse model catalyst (673 K, $p(\text{O}_2) = 4.7 \times 10^{-5}$ mbar), a total pressure of 0.2 mbar of CH_4 and CO_2 (1:1 ratio) was introduced into the HP cell at 673 K (figure 5).

Upon exposing the surface to the reactive gas atmosphere, the Zr 3d signal shifted from 181.7 to 181.9 eV. A similar

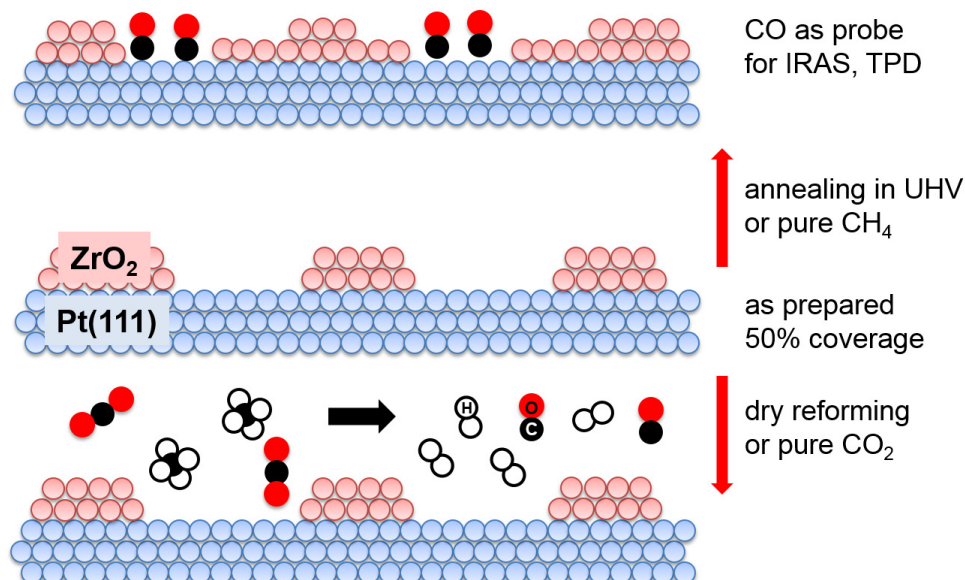


Figure 6. Scheme illustrating the $\text{ZrO}_2/\text{Pt}(111)$ inverse model catalyst surface during the different experiments.

small shift was observed in the O 1s spectra (529.3/530.3–529.6/530.6 eV). As discussed earlier, the reason for the peak shifts of Zr 3d and O 1s is a removal of surface/interface oxygen species from the ZrO_2 particle/island surface. For the dry reforming reaction the peak shift—and the intensity change of the ‘dynamic’ high BE O 1s compound (green)—is not as pronounced as for pure CH_4 because a 1:1 mixture of CH_4 and CO_2 was used. The gas atmosphere has therefore less reducing potential due to oxygen supply by CO_2 . Prior and during exposure to $\text{CH}_4 + \text{CO}_2$ mixture, no carbon signal was observed in the C 1s spectra, and the Pt 4f signal remained at 71 eV. When increasing the reaction temperature to 773 and 873 K no further changes appeared in the Zr 3d, C 1s and Pt 4f spectra. Only the high binding energy component of the O 1s signal slightly shifted by 0.1 eV to 530.6 eV. These observations indicate that the ZrO_2 particles were stable during reaction up to 873 K. There was no formation of a ZrO_2 ultrathin film wetting the Pt surface and thus no change in the amount of (reactive) sites. This shows that, at least under the applied conditions, no strong metal-support interaction (in the form of oxide wetting) occurred. Also, the surface stayed free of carbon deposits that would reduce the catalytic performance (a well-known effect especially for Ni catalysts). Only at lower reaction temperature (below ~ 500 K) carbon formation was observed. When the reaction temperature was raised from 773 to 873 K, mass spectroscopy detected minimal levels of CO/ H_2 (not shown) but the active surface area of the inverse model catalyst ($\sim 1 \text{ cm}^2$) was too small for meaningful acquisition of catalytic data in the BESSY II Setup.

4. Discussion

The current UHV and *in situ* NAP-XPS studies of an inverse model catalyst of ZrO_2 nanoislands on Pt(111) have shown that reducing conditions (UHV or CH_4) lead to the formation of an ultrathin ZrO_2 trilayer film partially covering the active

Pt(111) surface. A schematic of the observed processes is presented in figure 6.

This relates our study to technological applications, as SMSI upon reduction in hydrogen can lead to an increase or loss of catalytic activity, depending on reduction temperature [45, 46, 77]. A rational explanation is that at increasing reduction temperatures the noble metals are successively covered due to the overgrowth of thin oxide layers (often considered as sub-oxides originating from the support) [78–81]. In the initial stages, this may create additional active metal-oxide interfaces [82] but with successive encapsulation the metal may be fully blocked [83, 84]. Along these lines, Stagg-Williams *et al* demonstrated that Pt/ ZrO_2 catalysts reduced at 473 K showed higher activity for MDR than the catalyst reduced at 773 K [85]. Similarly, Faroldi *et al* highlighted for dry reforming on Ru/ $\text{La}_2\text{O}_3\text{-SiO}_2$ that reduction at 673 K induced higher activity than reduction at 823 K of the same catalyst [86]. Thus, for activation of noble metal catalysts, oxidation is typically followed by low temperature reduction.

Interestingly, also in the case of our inverse model catalyst, reducing conditions (UHV or CH_4) initiated SMSI, whereas (pure) CO_2 and the reaction environment (CO_2/CH_4 1:1 mixture) had a stabilizing effect on the ZrO_2 particle structure (and surface/interface oxygen), preventing the formation of a wetting ultrathin ZrO_2 film, thus preserving the active Pt surface area. Furthermore, during MDR at 673–873 K the surface remained free of any carbon deposits due to efficient carbon removal by CO_2 via the Boudouard reaction.

5. Conclusions

An inverse model catalyst of ZrO_2 clusters/islands supported on Pt(111) has been characterized after oxidation, when exposed to the individual reactants (CH_4 or CO_2) and *in situ* during the MDR reaction up to 873 K. The XPS data indicated that the ZrO_2 particles were reversibly wetting the Pt surface

upon annealing (reduction) in UHV or under reducing (CH_4) conditions, via the formation of an ultrathin ZrO_2 trilayer film. Upon reoxidation in O_2 the initial ZrO_2 particle structure and surface/interface oxygen were reestablished. Infrared spectroscopy of the probe molecule CO adsorbed on Pt(1 1 1) was used for confirmation, as the on-top CO signal reversibly diminished and reappeared upon UHV annealing and reoxidation, respectively.

Exposure to pure CH_4 at reaction temperatures led to the formation of carbon deposits. By switching to pure CO_2 the surface carbon was easily removed via the Boudouard reaction. For the actual MDR reaction (CH_4/CO_2 1:1) the $\text{ZrO}_2/\text{Pt}(1\ 1\ 1)$ inverse model catalyst was stable from 673 to 873 K. The Pt surface remained free of carbon and ZrO_2 remained in its oxidized state and island structure. In comparison to reducing UHV and pure CH_4 atmosphere, for which the formation of a wetting ZrO_2 trilayer film was observed, the dry reforming reaction environment was stabilizing the catalyst surface structure, preventing any SMSI effect to occur.

Acknowledgment

This work was supported by the Austrian Science Fund (FWF) through SFB 'FOXSI' F4502, Project DryRef (I 942-N17), and DK 'Solids4Fun' W1243, and through the European Community's Seventh Framework Programme (FP7/2007–2013) under grant agreement no. 312284. The authors gratefully acknowledge HZB/BESSY II for providing beamtime at the ISSS beamline and BESSY II staff for continuous support during beamtime. We also want to thank MAX IV Laboratory for providing beamtime at the SPECIES beamline and its staff for continuous support.

ORCID iDs

C Rameshan  <https://orcid.org/0000-0002-6340-4147>

G Rupprechter  <https://orcid.org/0000-0002-8040-1677>

References

- [1] Pakhare D and Spivey J 2014 A review of dry (CO_2) reforming of methane over noble metal catalysts *Chem. Soc. Rev.* **43** 7813–37
- [2] De Oliveira M E D, Vaughan B E and Rykiel E J 2005 Ethanol as fuels: energy, carbon dioxide balances, and ecological footprint *Bioscience* **55** 593–602
- [3] Usman M, Daud W and Abbas H F 2015 Dry reforming of methane: influence of process parameters—a review *Renew. Sustain. Energy Rev.* **45** 710–44
- [4] Schlogl R 2016 Sustainable energy systems: the strategic role of chemical energy conversion *Top. Catal.* **59** 772–86
- [5] Lunsford J H 2000 Catalytic conversion of methane to more useful chemicals and fuels: a challenge for the 21st century *Catal. Today* **63** 165–74
- [6] Rostrupnielsen J R 1993 Production of synthesis gas *Catal. Today* **18** 305–24
- [7] Pena M A, Gomez J P and Fierro J L G 1996 New catalytic routes for syngas and hydrogen production *Appl. Catal. A* **144** 7–57
- [8] Wilhelm D J, Simbeck D R, Karp A D and Dickenson R L 2001 Syngas production for gas-to-liquids applications: technologies, issues and outlook *Fuel Process. Technol.* **71** 139–48
- [9] Gangadharan P, Kanchi K C and Lou H H 2012 Evaluation of the economic and environmental impact of combining dry reforming with steam reforming of methane *Chem. Eng. Res. Des.* **90** 1956–68
- [10] Olah G A, Goepfert A, Czaun M and Prakash G K S 2013 Bi-reforming of methane from any source with steam and carbon dioxide exclusively to metgas (CO-2H(2)) for methanol and hydrocarbon synthesis *J. Am. Chem. Soc.* **135** 648–50
- [11] Larimi A S and Alavi S M 2012 Ceria–Zirconia supported Ni catalysts for partial oxidation of methane to synthesis gas *Fuel* **102** 366–71
- [12] Ruckenstein E and Hul Y H 1999 Methane partial oxidation over NiO MgO solid solution catalysts *Appl. Catal. A* **183** 85–92
- [13] Lucrecio A F, Assaf J M and Assaf E M 2012 Reforming of a model biogas on Ni and Rh–Ni catalysts: effect of adding La *Fuel Process. Technol.* **102** 124–31
- [14] Kohn M P, Castaldi M J and Farrauto R J 2014 Biogas reforming for syngas production: the effect of methyl chloride *Appl. Catal. B* **144** 353–61
- [15] Izquierdo U, Barrio V L, Requies J, Cambra J F, Guemez M B and Arias P L 2013 Tri-reforming: a new biogas process for synthesis gas and hydrogen production *Int. J. Hydrog. Energy* **38** 7623–31
- [16] Bradford M C J and Vannice M A 1999 CO_2 reforming of CH_4 *Catal. Rev.* **41** 1–42
- [17] Wurzel T, Malcus S and Mleczko L 2000 Reaction engineering investigations of CO_2 reforming in a fluidized-bed reactor *Chem. Eng. Sci.* **55** 3955–66
- [18] Chubb T A 1980 Characteristics of CO_2 – CH_4 reforming-methanation cycle relevant to the solchem thermochemical power system *Sol. Energy* **24** 341–5
- [19] Fraenkel D, Levitan R and Levy M 1986 A solar thermochemical pipe based on the CO_2 – CH_4 (1-1) system *Int. J. Hydrog. Energy* **11** 267–77
- [20] Ross J R H 2005 Natural gas reforming and CO_2 mitigation *Catal. Today* **100** 151–8
- [21] Cui Y H, Zhang H D, Xu H Y and Li W Z 2007 Kinetic study of the catalytic reforming of CH_4 with CO_2 to syngas over Ni/ α - Al_2O_3 catalyst: the effect of temperature on the reforming mechanism *Appl. Catal. A* **318** 79–88
- [22] Daza C E, Gallego J, Moreno J A, Mondragon F, Moreno S and Molina R 2008 CO_2 reforming of methane over Ni/Mg/Al/Ce mixed oxides *Catal. Today* **133** 357–66
- [23] Dimitrijewits M I, Guraya M M, Arciprete C P, Luna A C and Becerra A 2001 Catalytic behaviour Ni/(γ)- Al_2O_3 microporous catalysts in the methane dry-reforming reaction *Granular Matter* **3** 101–4
- [24] Abreu C A M, Santos D A, Pacifico J A and Lima N M 2008 Kinetic evaluation of methane-carbon dioxide reforming process based on the reaction steps *Ind. Eng. Chem. Res.* **47** 4617–22
- [25] Anic K, Wolfbeisser A, Li H, Rameshan C, Föttinger K, Bernardi J and Rupprechter G 2016 Surface spectroscopy on UHV-grown and technological Ni– ZrO_2 reforming catalysts: from UHV to operando conditions *Top. Catal.* **59** 1614–27
- [26] Asencios Y J O and Assaf E M 2013 Combination of dry reforming and partial oxidation of methane on NiO–MgO– ZrO_2 catalyst: effect of nickel content *Fuel Process. Technol.* **106** 247–52
- [27] Wolfbeisser A, Sopherphun O, Bernardi J, Wittayakun J, Föttinger K and Rupprechter G 2016 Methane dry

- reforming over ceria–zirconia supported Ni catalysts *Catal. Today* **277** 234–45
- [28] Bradford M C J and Vannice M A 1999 CO₂ reforming of CH₄ over supported Ru catalysts *J. Catal.* **183** 69–75
- [29] Mark M F and Maier W F 1996 CO₂-reforming of methane on supported Rh and Ir catalysts *J. Catal.* **164** 122–30
- [30] Munera J F, Irusta S, Cornaglia L M, Lombardo E A, Cesar D V and Schmal M 2007 Kinetics and reaction pathway of the CO₂ reforming of methane on Rh supported on lanthanum-based solid *J. Catal.* **245** 25–34
- [31] O'Connor A M, Schuurman Y, Ross J R H and Mirodatos C 2006 Transient studies of carbon dioxide reforming of methane over Pt/ZrO₂ and Pt/Al₂O₃ *Catal. Today* **115** 191–8
- [32] Nagaoka K, Seshan K, Lercher J A and Aika K 2000 Activation mechanism of methane-derived coke (CH_x) by CO₂ during dry reforming of methane—comparison for Pt/Al₂O₃ and Pt/ZrO₂ *Catal. Lett.* **70** 109–16
- [33] Demoulin O, Rupprechter G, Seunier I, Le Clef B, Navez M and Ruiz P 2005 Investigation of parameters influencing the activation of a Pd/gamma-alumina catalyst during methane combustion *J. Phys. Chem. B* **109** 20454–62
- [34] Kung K Y, Chen P, Wei F, Rupprechter G, Shen Y R and Somorjai G A 2001 Ultrahigh vacuum high-pressure reaction system for 2-infrared 1-visible sum frequency generation studies *Rev. Sci. Instrum.* **72** 1806–9
- [35] Nemeth M, Schay Z, Sranko D, Karolyi J, Safran G, Sajo I and Horvath A 2015 Impregnated Ni/ZrO₂ and Pt/ZrO₂ catalysts in dry reforming of methane: activity tests in excess methane and mechanistic studies with labeled (CO₂)-C-13 *Appl. Catal. A* **504** 608–20
- [36] Ocsachoque M, Pompeo F and Gonzalez G 2011 Rh–Ni/CeO₂–Al₂O₃ catalysts for methane dry reforming *Catal. Today* **172** 226–31
- [37] Wolfbeisser A, Kovacs G, Kozlov S M, Föttinger K, Bernardi J, Klotzer B, Neyman K M and Rupprechter G 2017 Surface composition changes of CuNi–ZrO₂ during methane decomposition: an operando NAP-XPS and density functional study *Catal. Today* **283** 134–43
- [38] Wolfbeisser A, Klotzer B, Mayr L, Rameshan R, Zemlyanov D, Bernardi J, Föttinger K and Rupprechter G 2015 Surface modification processes during methane decomposition on Cu-promoted Ni–ZrO₂ catalysts *Catal. Sci. Technol.* **5** 967–78
- [39] Föttinger K and Rupprechter G 2014 *In situ* spectroscopy of complex surface reactions on supported Pd–Zn, Pd–Ga, and Pd(Pt)–Cu nanoparticles *Acc. Chem. Res.* **47** 3071–9
- [40] Fuhrmann T, Kinne M, Whelan C M, Zhu J F, Denecke R and Steinrück H P 2004 Vibrationally resolved *in situ* XPS study of activated adsorption of methane on Pt(1 1 1) *Chem. Phys. Lett.* **390** 208–13
- [41] Bitter J H, Seshan K and Lercher J A 1998 Mono and bifunctional pathways of CO₂/CH₄ reforming over Pt and Rh based catalysts *J. Catal.* **176** 93–101
- [42] Ferreira-Aparicio P, Rodriguez-Ramos I, Anderson J A and Guerrero-Ruiz A 2000 Mechanistic aspects of the dry reforming of methane over ruthenium catalysts *Appl. Catal. A* **202** 183–96
- [43] Wei J M and Iglesia E 2004 Isotopic and kinetic assessment of the mechanism of reactions of CH₄ with CO₂ or H₂O to form synthesis gas and carbon on nickel catalysts *J. Catal.* **224** 370–83
- [44] Bradford M C J and Vannice M A 1996 Catalytic reforming of methane with carbon dioxide over nickel catalysts 1. Catalyst characterization and activity *Appl. Catal. A* **142** 73–96
- [45] Wang D, Penner S, Su D S, Rupprechter G, Hayek K and Schlogl R 2003 Silicide formation on a Pt/SiO₂ model catalyst studied by TEM, EELS, and EDXS *J. Catal.* **219** 434–41
- [46] Penner S, Wang D, Su D S, Rupprechter G, Podloucky R, Schlogl R and Hayek K 2003 Platinum nanocrystals supported by silica, alumina and ceria: metal-support interaction due to high-temperature reduction in hydrogen *Surf. Sci.* **532** 276–80
- [47] Hayek K, Fuchs M, Klotzer B, Reichl W and Rupprechter G 2000 Studies of metal-support interactions with ‘real’ and ‘inverted’ model systems: reactions of CO and small hydrocarbons with hydrogen on noble metals in contact with oxides *Top. Catal.* **13** 55–66
- [48] Rupprechter G 2007 A surface science approach to ambient pressure catalytic reactions *Catal. Today* **126** 3–17
- [49] Rupprechter G 2007 Sum frequency generation and polarization-modulation infrared reflection absorption spectroscopy of functioning model catalysts from ultrahigh vacuum to ambient pressure *Adv. Catal.* **51** 133–263
- [50] Rupprechter G 2001 Surface vibrational spectroscopy from ultrahigh vacuum to atmospheric pressure: adsorption and reactions on single crystals and nanoparticle model catalysts monitored by sum frequency generation spectroscopy *Phys. Chem. Chem. Phys.* **3** 4621–32
- [51] Rupprechter G, Dellwig T, Unterhalt H and Freund H J 2001 High-pressure carbon monoxide adsorption on Pt(1 1 1) revisited: a sum frequency generation study *J. Phys. Chem. B* **105** 3797–802
- [52] Mayr L, Koepfle N, Auer A, Klotzer B and Penner S 2013 An (ultra) high-vacuum compatible sputter source for oxide thin film growth *Rev. Sci. Instrum.* **84** 094103
- [53] Li H, Choi J-I J, Mayr-Schmoelzer W, Weilach C, Rameshan C, Mittendorfer F, Redinger J, Schmid M and Rupprechter G 2015 Growth of an ultrathin zirconia film on Pt₃Zr examined by high-resolution x-ray photoelectron spectroscopy, temperature-programmed desorption, scanning tunneling microscopy, and density functional theory *J. Phys. Chem. C* **119** 2462–70
- [54] Lackner P, Choi J I J, Diebold U and Schmid M 2017 Construction and evaluation of an ultrahigh-vacuum-compatible sputter deposition source *Rev. Sci. Instrum.* **88** 103904
- [55] Hollins P 2000 Infrared reflection–absorption spectroscopy *Encyclopedia of Analytical Chemistry* (New York: Wiley)
- [56] Michael H 2016 Innovative station for *in situ* spectroscopy www.helmholtz-berlin.de/pubbin/igama_output?modus=einzel&sprache=en&gid=1671
- [57] Schnadt J 2012 The new ambient-pressure x-ray photoelectron spectroscopy instrument at MAX-lab *J. Synchrotron Radiat.* **19** 701–4
- [58] Urpelainen S et al 2017 The SPECIES beamline at the MAX IV Laboratory: a facility for soft x-ray RIXS and APXPS *J. Synchrotron Radiat.* **24** 344–53
- [59] NIST Electron Effective-Attenuation-Length Database The National Institute of Standards and Technology (NIST) www.nist.gov/srd/nist82.cfm
- [60] Rameshan C, Ng M L, Shavorskiy A, Newberg J T and Bluhm H 2015 Water adsorption on polycrystalline vanadium from ultra-high vacuum to ambient relative humidity *Surf. Sci.* **641** 141–7
- [61] Gao Y, Zhang L, Pan Y, Wang G, Xu Y, Zhang W and Zhu J 2011 Epitaxial growth of ultrathin ZrO₂(1 1 1) films on Pt(1 1 1) *Chin. Sci. Bull.* **56** 502–7
- [62] Choi J I J, Mayr-Schmoelzer W, Mittendorfer F, Redinger J, Diebold U and Schmid M 2014 The growth of ultra-thin zirconia films on Pd₃Zr(000 1) *J. Phys.: Condens. Matter* **26** 225003
- [63] Antlanger M, Mayr-Schmoelzer W, Pavelec J, Mittendorfer F, Redinger J, Varga P, Diebold U and Schmid M 2012 Pt₃Zr(000 1): a substrate for growing well-ordered ultrathin zirconia films by oxidation *Phys. Rev. B* **86** 035451

- [64] Hayden B E and Bradshaw A M 1983 The adsorption of CO on Pt(1 1 1) studied by infrared reflection-absorption spectroscopy *Surf. Sci.* **125** 787–802
- [65] Rupprechter G, Dellwig T, Unterhalt H and Freund H J 2001 CO adsorption on Ni(100) and Pt(1 1 1) studied by infrared-visible sum frequency generation spectroscopy: design and application of an SFG-compatible UHV-high-pressure reaction cell *Top. Catal.* **15** 19–26
- [66] Starr D E, Wong E K, Worsnop D R, Wilson K R and Bluhm H 2008 A combined droplet train and ambient pressure photoemission spectrometer for the investigation of liquid/vapor interfaces *Phys. Chem. Phys.* **10** 3093–8
- [67] Binnig G, Quate C F and Gerber C 1986 Atomic force microscope *Phys. Rev. Lett.* **56** 930–3
- [68] Rameshan C *et al* 2010 Subsurface-controlled CO₂ selectivity of PdZn near-surface alloys in H₂ generation by methanol steam reforming *Angew. Chem., Int. Ed.* **49** 3224–7
- [69] Miller D J, Oberg H, Kaya S, Casalongue H S, Friebel D, Anniyev T, Ogasawara H, Bluhm H, Pettersson L G M and Nilsson A 2011 Oxidation of Pt(1 1 1) under near-ambient conditions *Phys. Rev. Lett.* **107** 195502
- [70] Bukhtiyarov V I and Kaichev V V 2000 The combined application of XPS and TPD to study of oxygen adsorption on graphite-supported silver clusters *J. Mol. Catal. A* **158** 167–72
- [71] Do Y, Choi J S, Kim S K and Sohn Y 2010 The interfacial nature of TiO₂ and ZnO nanoparticles modified by gold nanoparticles *Bull. Korean Chem. Soc.* **31** 2170–4
- [72] Norton P R, Goodale J W and Selkirk E B 1979 Adsorption of CO on Pt(1 1 1) studied by photoemission, thermal-desorption spectroscopy and high-resolution dynamic measurements of work function *Surf. Sci.* **83** 189–227
- [73] Petersen M A, Jenkins S J and King D A 2004 Theory of methane dehydrogenation on Pt{1 1 0}(1 × 2). Part 1: chemisorption of CH_x (x = 0–3) *J. Phys. Chem. B* **108** 5909–19
- [74] Fuhrmann T, Kinne M, Trankenschuh B, Papp C, Zhu J F, Denecke R and Steinruck H P 2005 Activated adsorption of methane on Pt(1 1 1)—an *in situ* XPS study *New J. Phys.* **7** 1–19
- [75] Souza M and Schmal M 2003 Methane conversion to synthesis gas by partial oxidation and CO₂ reforming over supported platinum catalysts *Catal. Lett.* **91** 11–7
- [76] Qin D and Lapszewicz J 1994 Study of mixed steam and CO₂ reforming of CH₄ to syngas on MgO-supported metals *Catal. Today* **21** 551–60
- [77] Hayek K, Goller H, Penner S, Rupprechter G and Zimmermann C 2004 Regular alumina-supported nanoparticles of iridium, rhodium and platinum under hydrogen reduction: structure, morphology and activity in the neopentane conversion *Cata. Lett.* **92** 1–9
- [78] Rupprechter G, Seeber G, Goller H and Hayek K 1999 Structure-activity correlations on Rh/Al₂O₃ and Rh/TiO₂ thin film model catalysts after oxidation and reduction *J. Catal.* **186** 201–13
- [79] Tauster S J and Fung S C 1978 Strong metal-support interactions—occurrence among binary oxides of groups IIA–VB *J. Catal.* **55** 29–35
- [80] Unterberger W, Jenewein B, Klotzer B, Penner S, Reichl W, Rupprechter G, Wang D, Schlogl R and Hayek K 2006 Hydrogen-induced metal-oxide interaction studied on noble metal model catalysts *React. Kinetics Catal. Lett.* **87** 215–34
- [81] Fuchs M, Jenewein B, Penner S, Hayek K, Rupprechter G, Wang D, Schlogl R, Calvino J J and Bernal S 2005 Interaction of Pt and Rh nanoparticles with ceria supports: ring opening of methylcyclobutane and CO hydrogenation after reduction at 373–723 K *Appl. Catal. A* **294** 279–89
- [82] Suchorski Y *et al* 2018 The role of metal/oxide interfaces for long-range metal particle activation during CO oxidation *Nat. Mater.* **17** 519–22
- [83] Pesty F, Steinruck H P and Madey T E 1995 Thermal-stability of Pt films on TiO₂(1 1 0)—evidence for encapsulation *Surf. Sci.* **339** 83–95
- [84] Dulub O, Hebenstreit W and Diebold U 2000 Imaging cluster surfaces with atomic resolution: the strong metal-support interaction state of Pt supported on TiO₂(1 1 0) *Phys. Rev. Lett.* **84** 3646–9
- [85] Stagg-Williams S M, Noronha F B, Fendley G and Resasco D E 2000 CO₂ reforming of CH₄ over Pt/ZrO₂ catalysts promoted with La and Ce oxides *J. Catal.* **194** 240–9
- [86] Faroldi B M, Lombardo E A and Cornaglia L M 2009 Surface properties and catalytic behavior of Ru supported on composite La₂O₃–SiO₂ oxides *Appl. Catal. A* **369** 15–26